www.sciencemag.org/cgi/content/full/science.aaf5206/DC1

Supplementary Materials for

De novo synaptogenesis induced by GABA in the developing mouse cortex

Won Chan Oh, Stefano Lutzu, Pablo E. Castillo, Hyung-Bae Kwon*

*Corresponding author. E-mail: hyungbae.kwon@mpfi.org

Published 11 August 2016 on *Science* First Release
DOI: 10.1126/science.aaf5206

This PDF file includes:

Other supplementary material for this manuscript includes:

Movies S1 and S2

Materials and Methods

Preparation and transfection of organotypic cortical slice cultures. Organotypic slice cultures from mouse somatosensory cortex were prepared from postnatal day 1 (P1)-P3 mice, as described previously (*30*), in accordance with the Institutional Animal Care and Use of Max Planck Florida Institute for Neuroscience and National Institutes of Health guidelines. Mice were acquired from Charles River Laboratory (C57BL/6 wild type) and Jackson Laboratory [SOM-Cre (13044), PV-Cre (8069)]. Slices were transfected 2-3 days (tdTomato, Dio-Teal-gephyrin, and Cre) or 6-8 days (tdTomato, SypHy A4, Flex-tetanus toxin light-chain, Cre) prior to imaging using biolistic gene transfer (180 psi). A total of 12 μg of tdTomato (*31*), 18 μg of Dio-Teal-gephyrin (gift from Elly Nedivi (*10*)), and 16 μg of Cre (gift from Elly Nedivi (*10*)) or 12 μg of tdTomato, 20 μg of CMV::SypHy A4 [gift from Leon Lagnado (Addgene plasmid # 24478) (*32*)], 20 μg of Flex-tetanus toxin light-chain (gift from Hiroki Taniguchi, Max Planck Florida Institute for Neuroscience), and 16 μg of Cre were coated onto 6-7 mg of gold particles. 10 μg of pGP-CMV-GCaMP6s [gift from Douglas Kim (Addgene plasmid # 40753) (*33*)] was added, when needed. The age of the culture is reported as equivalent postnatal (EP) day; postnatal day at slice culturing + days *in vitro*.

Preparation of acute cortical slices. Acute coronal cortical slices were prepared from C57BL/6 wild type mice, P6-24, either gender, in accordance with the Institutional Animal Care and Use of Max Planck Florida Institute for Neuroscience, the Albert Einstein College of Medicine Institutional Animal Care and Use Committee, and National Institute of Health guidelines. Mice were anesthetized with isoflurane and killed by decapitation. The brain was removed from the skull and rapidly placed in ice-cold cutting solution containing (in mM): 215 sucrose, 20 glucose, 26 $NaHCO_3$, 4 $MgCl_2$, 4 $MgSO_4$, 1.6 NaH_2PO_4, 1 $CaCl_2$ and 2.5 KCl. Cortical slices (400 μm thick) were prepared using a VT1000S or 1200S vibrating microtome (Leica). Slices were incubated at 32 °C for 30 minutes in a holding chamber containing 50% cutting solution and 50% artificial cerebrospinal fluid (ACSF) containing (in mM): 124 NaCl, 26 $NaHCO_3$, 10 glucose, 2.5 KCl, 1 NaH_2PO_4, 2.5 $CaCl_2$, and 1.3 $MgSO_4$. After 30 minutes, this solution was slowly replaced with ACSF at room temperature. Slices were allowed to recover for 1 hour in ACSF before recording. For electrophysiology experiments slices were transferred to a

submersion-type, temperature-controlled recording chamber (TC-344B, Warner Instruments) and perfused with ACSF. Recordings were performed at 26 °C. All solutions were equilibrated for at least 30 min with 95%O_2/5%CO_2.

Virus infection of organotypic cortical slice cultures. Slices were infected by adding a 5 µl of solution containing 1 µl of concentrated virus (titer: ~10^{12}-10^{13} GC/ml) and 4 µl of slice culture media (pre-warmed at 37 °C) to the top of the cortical layers of brain slices as a drop with a micropipette. Pipette approached the tissue at an angle as steep to the plane of the brain slice as possible for large-scale infection with maximal delivery of fluid while minimizing pipetting time (< 1 min). After infection, slices were returned to the incubator (37 °C) and multiple infections (2-3 times a week) were made prior to experiments to allow persistent expression of viral gene products. To achieve expression of channelrhodopsin-2, tetanus toxin light-chain, GCaMP6s, tdTomato, and Cre, AAV1-EF1-dflox-hChR2(H134R)-mCherry-WPRE-hGH, AAV-CAG-Flex-tetanus toxin light-chain (produced from ViGene Biosciences, MD), AAV1-Syn-GCaMP6s-WPRE-SV40, AAV1-CAG-Flex-tdTomato-WPRE-bGH, and AAV1-CMV-PI-Cre-rBG were used, respectively. All viruses were purchased from the viral vector cores of the University of Pennsylvania unless otherwise noted.

Two-photon imaging. Imaging was performed at 2-15 days *in vitro* (DIV) on transfected layer 2/3 pyramidal neurons within 40 µm of the slice surface at 30 °C in recirculating ACSF (in mM: 127 NaCl, 25 $NaHCO_3$, 1.25 NaH_2PO_4, 2.5 KCl, 25 D-glucose, aerated with 95%O_2/5%CO_2). For each neuron, image stacks (512 × 512 pixels; 0.035 µm / pixel) with 1-µm z-steps were collected from one segment of secondary or tertiary apical and/or basal dendrites using a two-photon microscope (Prairie Technologies, Inc) with a pulsed Ti::sapphire laser (MaiTai HP DeepSee, Spectra Physics) tuned to 920 nm (2-2.5 mW at the sample) or a HighQ-2 laser (Spectra Physics) tuned to 1,045 nm (5-7 mW at the sample). All images shown are maximum projections of 3D image stacks after applying a median filter (2 × 2) to the raw image data.

High-frequency uncaging stimulus. Two-photon uncaging was achieved, as previously described (*9, 34*), except that CDNI-GABA and CDNI-glutamate were used. In brief, both GABA and glutamate high-frequency uncaging (HFU) stimuli consisted of 60 pulses (720 nm;

14-15 mW at the sample) of 2-ms duration delivered at 10 Hz by parking the beam at a point ~0.5 μm from the edge of a dendrite with a pulsed Ti::sapphire laser (MaiTai HP, Spectra-Physics). Imaging-only experiments to induce *de novo* synaptogenesis were carried out at 30 °C in ACSF containing (in mM): 2 Ca^{2+}, 1 Mg^{2+}, 0.001 TTX, and 0.5 CDNI-GABA or 2 Ca^{2+}, 0 Mg^{2+}, 0.001 TTX, and 2.5 CDNI-glutamate. No more than three synaptogenesis trials were performed from the same neuron. The mock stimulus was identical in parameters to the HFU stimulus, except carried out in the absence of caged compounds. For NPEC-caged-D-AP5 photolysis, 0.5 mM concentration was perfused into a slice chamber. Electrophysiology experiments to assess the accumulation of functional $GABA_A$ receptors at newly formed Teal-gephyrin puncta were carried out at 25 °C in ACSF containing (in mM): 2 Ca^{2+}, 1 Mg^{2+}, 0.001 TTX, and 0.5 CDNI-GABA. To examine the accumulation of functional glutamate receptors at newly formed spines, *de novo* spinogenesis was induced by GABA HFU as described above and new ACSF was washed in (in mM: 2 Ca^{2+}, 1 Mg^{2+}, 0.001 TTX, and 2.5-3 MNI-glutamate).

Electrophysiology. Whole-cell recordings (electrode resistances 5-8 MΩ; series resistances 20-40 MΩ) were performed at 25 °C on visually identified layer 2/3 pyramidal neurons within 40 μm of the slice surface using a MultiClamp 700B amplifier (Molecular Devices). To record uncaging-evoked inhibitory postsynaptic currents (uIPSCs), layer 2/3 pyramidal neurons were patched in voltage-clamp configuration (Vhold = +10 mV) using cesium-based internal solution (in mM: 135 Cs-methanesulfonate, 10 HEPES, 10 Na_2 phosphocreatine, 4 $MgCl_2$, 4 Na_2-ATP, 0.4 Na-GTP, 3 Na L-ascorbate, 0.02 Alexa 594, ~300 mOsm, ~pH 7.25) in ACSF containing (in mM): 2 Ca^{2+}, 1 Mg^{2+}, 0.001 TTX, and 1 CDNI-GABA. 720 nm light was delivered at ~0.5 μm away from the edge of a dendrite with a power of 18-20 mW for 3-ms duration. uIPSC amplitudes were quantified as the average (8-10 test pulses at 0.1 Hz) from a 2-ms window centered on the maximum current amplitude within 50 ms after uncaging pulse delivery. To assess functional properties of the newly formed Teal-gephyrin puncta, uIPSCs were acquired in ACSF (2 mM Ca^{2+}, 1 mM Mg^{2+}, 0.001 mM TTX, and 0.5 mM CDNI-GABA) from one target and one neighboring region on the same dendritic segment. To avoid confounds due to GABA spillover, neighboring regions that were located at least 4 μm away from targets were chosen. After a short baseline of uIPSCs, GABA HFU was delivered at the target while the cell was stepped from +10 to -65 mV. Post-HFU uIPSCs were recorded at +10 mV from both target and

neighboring regions at 7- to 8-min intervals. To assess functional properties of the newly formed dendritic spines, uncaging-evoked excitatory postsynaptic currents (uEPSCs) were recorded from new spines in voltage-clamp configuration (Vhold = -65 mV) using cesium-based internal solution in ACSF (2 mM Ca^{2+}, 1 mM Mg^{2+}, 0.001 mM TTX, and 2.5-3 mM MNI-glutamate). uEPSC amplitudes were quantified as the average (8-10 test pulses of 1-ms duration at 0.1 Hz) from a 2-ms window centered on the maximum current amplitude after uncaging pulse delivery. For spontaneous miniature inhibitory postsynaptic current (mIPSC) recording, layer 2/3 neurons were patched at 30 °C in voltage-clamp configuration (Vhold = +10 mV) using cesium-based internal solution in ACSF containing (in mM): 2 Ca^{2+}, 1 Mg^{2+}, 0.001 TTX, 0.01 CPP, and 0.01 NBQX. Spontaneous miniature excitatory postsynaptic current (mEPSC) was measured at 30 °C in voltage-clamp configuration (Vhold = -65 mV) using cesium-based internal solution in ACSF containing (in mM): 2 Ca^{2+}, 1 Mg^{2+}, 0.001 TTX, 0.01 CPP, and 0.01 Bicuculline. To monitor spiking properties, whole-cell properties were recorded in current-clamp mode using potassium-based internal solution (in mM: 136 K-gluconate, 10 HEPES, 17.5 KCl, 9 NaCl, 1 $MgCl_2$, 4 Na_2-ATP, 0.4 Na-GTP, and ~300 mOsm, ~pH 7.26) at 25 °C in ACSF containing 2 mM Ca^{2+} and 1 mM Mg^{2+}. To examine the effectiveness of CGP55845, after a 5 min baseline period, firing properties of recorded cells were monitored before and after CGP55845 application (3 μM) from neurons preincubated with baclofen (20 μM). For synaptic vesicle fusion experiments, a stimulus train of action potentials was evoked by 10 step current injections (200-300 pA, 50 ms) delivered at 2 Hz. Signals were filtered at 2 kHz and digitized at 10 kHz and responses were analyzed using Clampfit 10.3 (Molecular Devices) and OriginPro 8.5 software (OriginLab).
Perforated patch-clamp recordings (electrode resistances 2.5-4 MΩ) from layer 2/3 pyramidal neurons were performed using a MultiClamp 700B amplifier (Molecular Devices). Perforation was achieved using the antibiotic, gramicidin (stock concentration 5 mg/ml in DMSO) diluted to 30-60 μg/ml in a cesium-gluconate-based internal solution containing (in mM): 131 Cs-gluconate, 8 NaCl, 1 $CaCl_2$, 10 EGTA, 10 glucose, 10 HEPES, and ~pH 7.4. Glass pipettes were front-filled with normal internal solution, then backfilled with internal solution containing gramicidin. After obtaining a giga-Ohm seal, the series resistance was allowed to stabilize (range: 80-100 MΩ). In all cases the input resistance/series resistance was larger than 10. IPSCs were evoked using a patch-type pipette filled with extracellular solution, placed 80-100 μm from the soma, in the presence of AMPA/Kainate and NMDA receptor antagonists NBQX (10 μM)

and D-APV (25 µM), respectively. The $GABA_A$ receptor-mediated nature of the recorded IPSCs was tested by applying the $GABA_A$ receptor antagonist picrotoxin (100 µM). Cells were voltage-clamped at different potentials ranging from -90 to -30 mV. I-V relationships were plotted showing peak-IPSC at different voltages. The reversal potential was measured by calculating the intercept of the linear fit of the I-V curve with the x-axis. Junction potential was measured (-5.1 mV) and compensated. Signals were filtered at 2.4 kHz and acquired at 5 kHz with custom software written in IgorPro 5.05 (Wavemetrics) and analyzed using OriginPro 9.0 software (OriginLab). To measure the polarity of GABA uncaging-induced (1 pulse of 50-ms duration, 16-18 mW at the sample) membrane potential changes and to examine the resting membrane potentials, tight seal (>6 GΩ) cell-attached current-clamp recordings were performed (I=0) using potassium-based internal solution containing (in mM): 140 K-gluconate, 10 HEPES, 11 EGTA, 1 $CaCl_2$ and 2 $MgCl_2$, and ~297 mOsm, ~pH 7.25. Similar to the perforated patch-clamp recording, GABA reversal potential was measured by recording single $GABA_A$ channels using a GABA-containing internal solution (in mM): 120 NaCl, 20 tetraethylammonium chloride, 5 KCl, 5 4-aminopyridine, 0.1 $CaCl_2$, 10 $MgCl_2$, 10 glucose, 10 HEPES, 0.005 GABA, and ~298 mOsm, ~pH 7.26. Single channel signals were filtered at 2 kHz and digitized at 20 kHz.

Intracranial virus injection and *in vivo* two-photon imaging and uncaging. Viruses were injected into somatosensory cortex in a stereotactic setup (Kopf instruments, Tujunga, CA, USA). Neonate mice (P0-1) were cryoanesthetized. Following cessation of movement, a solution of recombinant AAV diluted in sterile phosphate-buffered saline was injected unilaterally into layer 2/3 somatosensory cortex using a pulled glass needle (30-40 µm). The needle was held perpendicular to the skull surface during insertion to a depth of approximately 200-300 µm. Once the needle was in place, 1-2 µl of viral solution was manually injected. 500-750 nl injections were used for Teal-gephyrin, tdTomato, and TeTxLC expression. 10 nl injection was used to drive Cre expression. After injection, pups were placed on a warming pad for recovery. Five to 12 days after viral injection, 2-3 mm craniotomy was made for imaging and uncaging. A customized anodized cone-shape *in vivo* chamber was attached to the skull around the craniotomy site and fixed by dental cement. *In vivo* chamber was firmly affixed to the head plate connected to the head post at the stage. Mice were anesthetized with the cocktail of ketamine and xylazine (0.1 mg/0.01 mg/g) during surgery and experiment. For *in vivo* two-photon GABA

uncaging, dura mater was carefully removed. *In vivo* GABA HFU stimuli consisted of 60 pulses (720 nm; 18-20 mW at the sample) of 5-ms duration delivered at 10 Hz. 10 mM CDNI-GABA containing ACSF was added into the *in vivo* chamber.

Quantification of densities and fluorescence intensities of dendritic spines. All distinct protrusions emanating from the dendritic shaft, regardless of shape, were counted and measured in images from the red (tdTomato) channel using ImageJ (NIH). For all cells included in our analysis, overall spine density did not significantly change over the 1 hour imaging session (data not shown). This ensured that the *de novo* spinogenesis being examined did not take place due to a general decrease in cell health, as widespread spine/filopodia-like structures can form when cell health is compromised. Estimated spine volume was measured from bleed-through-corrected and background-subtracted red fluorescence intensities using the integrated pixel intensity of a boxed region of interest (ROI) surrounding the spine head, as previously described (*34*, *35*).

Quantification of densities and fluorescence intensities of Teal-gephyrin puncta. Teal-gephyrin fluorescence intensities were calculated from bleed-through-corrected and background-subtracted green (Teal-gephyrin) fluorescence intensities using the integrated pixel intensity of a boxed region surrounding a Teal-gephyrin punctum, as previously described (*35*). In brief, Teal-gephyrin puncta whose green fluorescence intensities were higher than two standard deviations (2 SDs) of the local background green fluorescence levels measured from 2 ROIs near the puncta were recognized as true Teal-gephyrin puncta and counted in images from the green channel using ImageJ. "Teal-gephyrin puncta" (expression level > 2 SDs of background levels) *vs.* "No puncta" (expression level < 2 SDs of background levels). Teal-gephyrin enrichment in dendritic shafts was calculated by normalizing the Teal-gephyrin fluorescence intensities (as described above) for each individual punctum to the mean Teal-gephyrin fluorescence intensities measured from 4 ROIs on the same dendritic shaft.

Criteria for *de novo* formation of dendritic spines and Teal-gephyrin puncta. Only a new spine that grew during the initial 5 minute (*in vitro*) or 10 minute (*in vivo*) time-lapse period after HFU stimulus was considered HFU-induced *de novo* spine outgrowth. If there was uncertainty concerning the status of a new spine because of undulations in the dendrite, swellings in the z-

axis, or neighboring spine movement, the spine was excluded. For *de novo* Teal-gephyrin puncta formation, fold enrichment of Teal-gephyrin in dendritic shafts was calculated from bleed-through-corrected and background-subtracted green (Teal-gephyrin) and red (tdTomato) signal intensities in the dendrite at the site where the HFU stimulus was delivered by dividing the green signal by the red signal following the HFU (Green t2/Red t2) and normalizing to the green signal divided by the red signal at the first baseline time point imaged (Green t1/Red t1). Teal-gephyrin puncta were considered to have newly formed when the fold enrichment of green to red ratio [ΔG/R (%) = (Green t2/Red t2) / (Green t1/Red t1)] was higher than 114% (> average 2 SDs of green signal divided by red signal at resting state, n=14 cells) *in vitro* and 120% *in vivo* (n=18 cells). Only a new Teal-gephyrin punctum that formed during the initial 5 minute (*in vitro*) or 10 minute (*in vivo*) time-lapse period after HFU stimulus was considered HFU-induced *de novo* gephyrin puncta formation.

Calcium Imaging. Line-scan recording of Ca^{2+} transients was performed simultaneous with GABA uncaging on layer 2/3 pyramidal neurons using two pulsed Ti::sapphire lasers for imaging and uncaging at wavelengths of 920 nm and 720 nm, respectively, in ACSF containing (in mM): 4 Ca^{2+}, 1 Mg^{2+}, 0.001 TTX, 0.01 CPP, and 0.5 CDNI-GABA. The fluorescent measurements of Ca^{2+} transients were represented as $\Delta G/R = [(G/R)_{peak} / (G/R)_{baseline}]$, where G (green) is the GCaMP6s fluorescence and R (red) is tdTomato fluorescence. After measuring baseline fluorescences (50 ms), GABA uncaging (1 pulse of 6-ms duration, 14-15 mW) was delivered at the target region and peak fluorescences were averaged over 30 ms around the peak. Dark currents from the corresponding photomultipliers (PMTs) were subtracted from both green and red fluorescences and only cells that showed stable Ca^{2+}-insensitive (R) signals (< ±5% fluctuation) were included in our analysis (*36*).

Optogenetic stimulus. To examine spiking properties, AAV1-EF1-dflox-hChR2(H134R)-mCherry-WPRE-hGH expressing somatostatin cortical interneurons were visually identified and action potentials were measured by blue light illumination (10 pulses of 380-ms duration at 1 Hz, 450-480 nm, 3.4 mW). Signals were filtered at 2 kHz and digitized at 10 kHz and responses were analyzed using Clampfit 10.3 (Molecular Devices) and OriginPro 8.5 software (OriginLab). For *de novo* synaptogenesis experiments, two-photon imaging with a pulsed Ti::sapphire laser tuned

to 920 nm or a HighQ-2 laser tuned to 1,045 nm was performed on transfected layer 2/3 pyramidal neurons in ChR2 expressing SOM-Cre slices at 30 °C in ACSF containing (in mM): 2 Ca^{2+}, 1 Mg^{2+}. Image stacks with 1-μm z-steps were collected from one segment of secondary or tertiary distal apical dendrites > 100 μm from the soma before and after three trains of optical stimuli delivered at 0.1 Hz. Each optical stimulus consisted of 10 pulses of 380-ms duration delivered at 1 Hz.

Pharmacology. Stocks were prepared at 1,000 × (or greater) by dissolving Tetrodotoxin citrate, (R)-CPP, D-APV, (R)-Baclofen, Mibefradil dihydrochloride, Bicuculline methochloride, and GABAzine in water; NBQX, Nifedipine, CGP55845, Picrotoxin, Bumetanide, and Gramicidin (Santa Cruz Biotechnology) in DMSO. All drugs were from Tocris unless otherwise noted. Drugs tested for *de novo* synaptogenesis were applied at least 25 min prior to HFU stimulation.

Statistics. All statistics were calculated across cells. Error bars represent standard error of the mean and significance was set at $P = 0.05$ (Student's two-tailed t test). Comparison of reversal potentials was made by a non-parametric test (Mann-Whitney). Correlation was examined by Pearson's correlation. Success rate of *de novo* synaptogenesis across conditions was compared by Fisher's exact test (two-sided). Single and double asterisks indicate $P < 0.05$ and $P < 0.01$, respectively. n.s., not significant.

Fig. S1

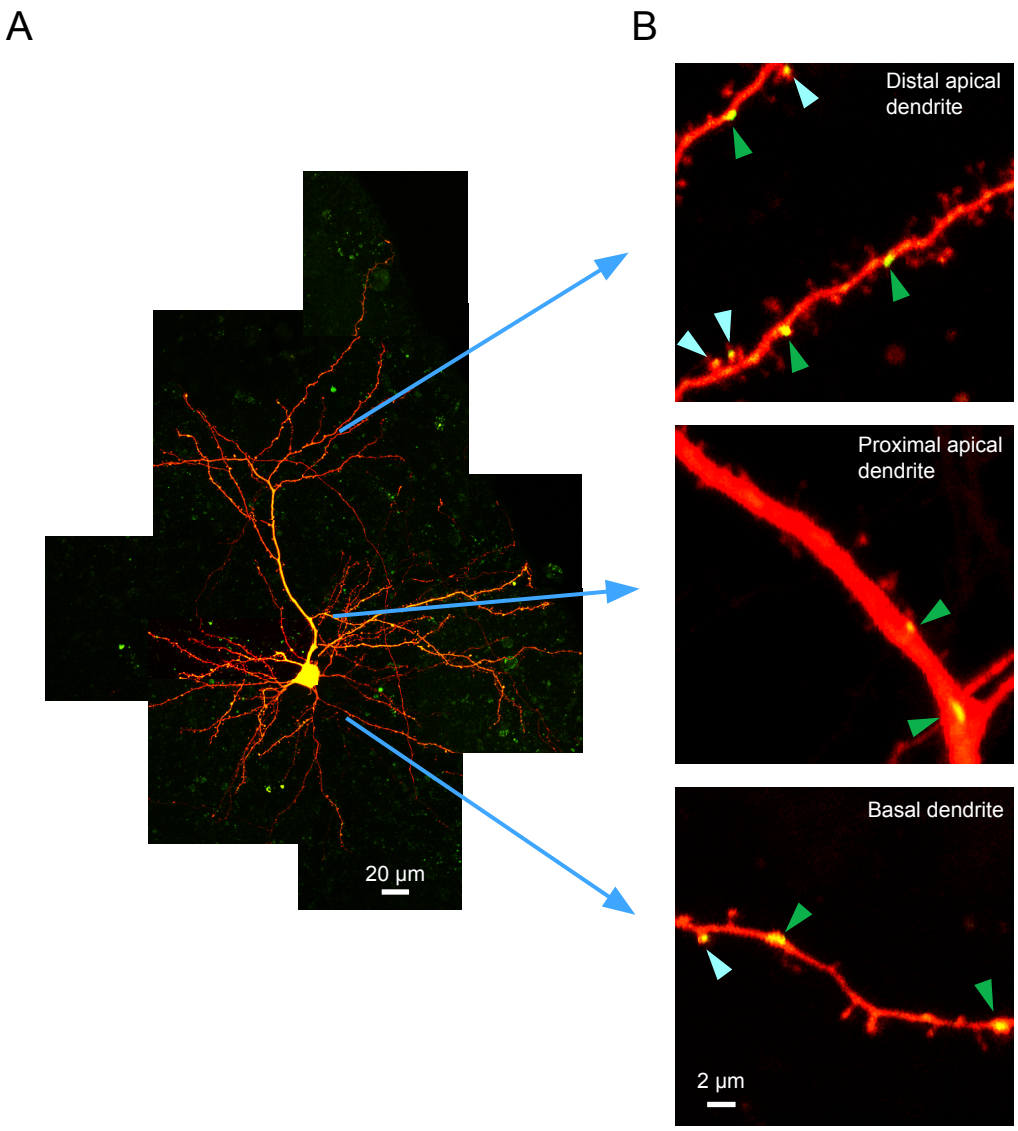

Fig. S1. Two-photon images of gephyrin puncta and dendritic spines in layer 2/3 pyramidal neurons of organotypic cortical slices. (**A**) Representative image of a layer 2/3 pyramidal neuron coexpressing Teal-gephyrin (green) and tdTomato (red) at 14 DIV. (**B**) Inhibitory synapses (Teal-gephyrin) and dendritic spines (tdTomato) were labelled on different dendritic branches of a layer 2/3 neuron. Teal-gephyrin puncta were clearly observed on dendritic shaft (inhibitory shaft synapses; green arrowheads) and on a subset of dendritic spines (inhibitory spine synapses; blue arrowheads).

Fig. S2

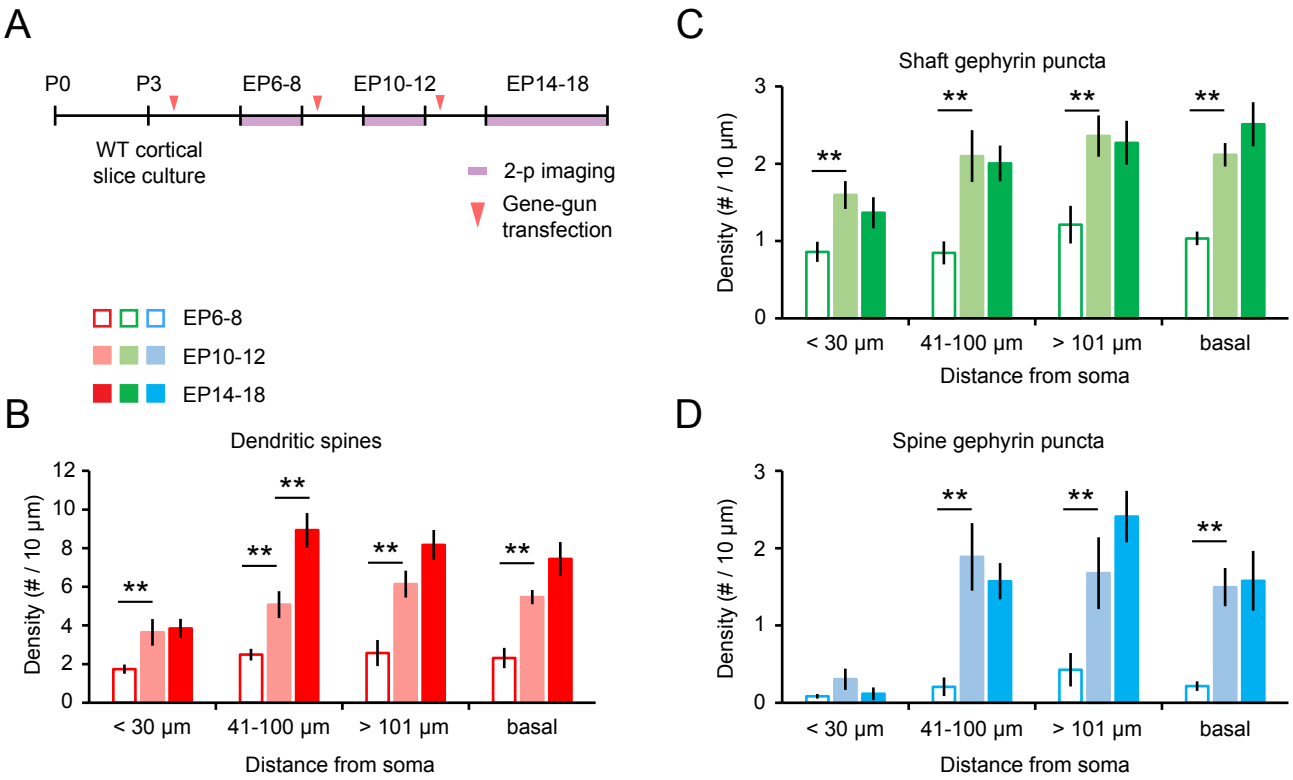

Fig. S2. Changes in the density of Teal-gephyrin puncta and dendritic spines of layer 2/3 pyramidal neurons in the somatosensory cortex across development. (**A**) Experimental timeline. P, postnatal day. EP, equivalent postnatal day (postnatal day at slice culturing + days *in vitro*). (**B**) Quantification of spine density over time on different sets of dendritic branches. Spine density significantly increased nearly twofold between EP6-8 (open bars; <30µm, 41-100µm, >101µm, basal: 1.74 ± 0.24, 2.49 ± 0.30, 2.58 ± 0.68, 2.31 ± 0.53) and EP10-12 (light filled bars; 3.65 ± 0.69, 5.08 ± 0.70, 6.14 ± 0.69, 5.47 ± 0.37) in culture and remained unchanged at EP14-18 (dark filled bars; 3.85 ± 0.49, 8.93 ± 0.89, 8.17 ± 0.77, 7.44 ± 0.87), except the 41-100 µm section of apical dendrites. (**C**) Quantification of shaft gephyrin puncta density on different dendritic branches across development. The density of shaft gephyrin puncta significantly increased nearly twofold at all dendritic branches between EP6-8 (0.86 ± 0.13, 0.85 ± 0.15, 1.21 ± 0.24, 1.03 ± 0.09) and EP10-12 (1.60 ± 0.18, 2.10 ± 0.34, 2.36 ± 0.27, 2.12 ± 0.15) and remained unchanged at EP14-18 (1.37 ± 0.20, 2.00 ± 0.23, 2.27 ± 0.28, 2.51 ± 0.29). (**D**) Quantitative analysis of gephyrin puncta density on dendritic spines over time on different sets of dendritic branches. The density of spine gephyrin puncta significantly increased between EP6-8 (0.09 ± 0.03, 0.21 ± 0.12, 0.43 ± 0.22, 0.22 ± 0.06) and EP10-12 (0.30 ± 0.14, 1.89 ± 0.44, 1.68 ± 0.46, 1.50 ± 0.25), but not between EP10-12 and EP14-18 (0.12 ± 0.08, 1.57 ± 0.23, 2.41 ± 0.33, 1.58 ± 0.39). Note that spine gephyrin puncta were rarely observed on proximal apical dendrites across development (on average n=9 dendritic branches per cell, 6 cells each age group). $^{**}P < 0.01$. Error bars represent s.e.m.

Fig. S3

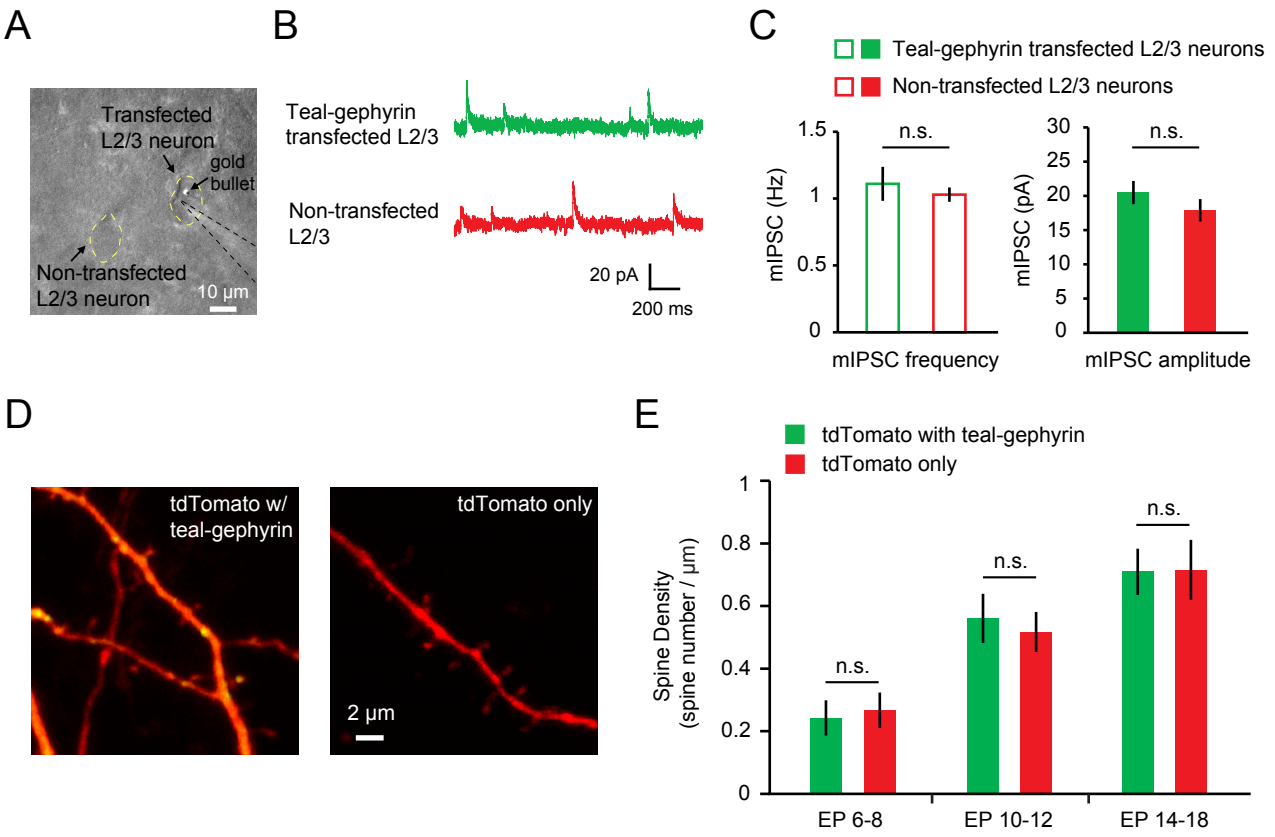

Fig. S3. Neither electrophysiological properties of inhibitory synapses nor excitatory synapse density are altered in layer 2/3 pyramidal neurons expressing low levels of Teal-gephyrin. (**A**) Representative DIC image of an organotypic cortical slice maintained in culture showing whole-cell recording from a Teal-gephyrin transfected cell (indicated by a gold bullet) and a control, neighboring cell. (**B**) Representative mIPSC traces from Teal-gephyrin transfected and non-transfected cells. (**C**) Both the frequency (open bars; gephyrin: 1.11 ± 0.13Hz; control: 1.03 ± 0.05Hz; $P = 0.54$) and amplitude (filled bars; gephyrin: 20.49 ± 1.69pA; control: 17.88 ± 1.65pA; $P = 0.30$) of mIPSCs were not significantly different between Teal-gephyrin transfected (green bars; n=8 cells) and non-transfected cells (red bars; n=10 cells). (**D**) Images of dendrites from a layer 2/3 neuron coexpressing Teal-gephyrin and tdTomato (left panel) and a control layer 2/3 neuron expressing tdTomato alone (right panel). (**E**) Spine density was not significantly different between cells expressing both Teal-gephyrin and tdTomato (green bars; EP6-8, EP10-12, EP14-18: 0.24 ± 0.06, 0.56 ± 0.08, 0.71 ± 0.07) and those expressing tdTomato alone (red bars; 0.27 ± 0.06, 0.52 ± 0.06, 0.72 ± 0.10) in three different age groups (n=8 cells each, EP6-8: $P = 0.62$; EP10-12: $P = 0.67$; EP14-18: $P = 0.97$). Error bars represent s.e.m.; n.s., not significant.

Fig. S4

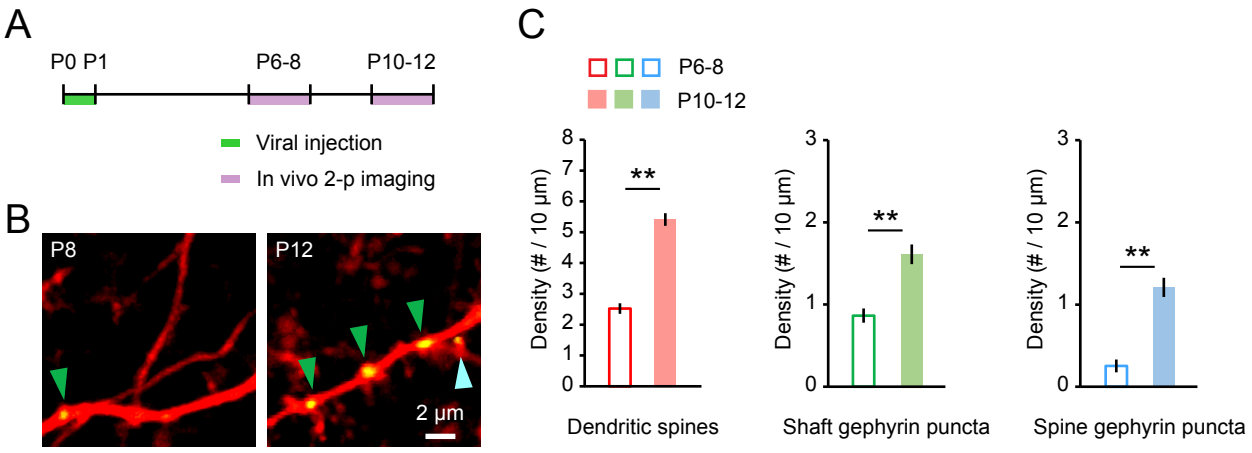

Fig. S4. *In vivo* imaging of dendritic spines and Teal-gephyrin puncta on distal apical dendrites of layer 2/3 pyramidal neurons in the somatosensory cortex during early development. (**A**) Experimental timeline. P, postnatal day. AAV1-CMV-PI-Cre-rBG, AAV1-CAG-Flex-Teal-gephyrin, and AAV1-CAG-Flex-tdTomato-WPRE-bGH were injected into somatosensory cortex of WT at P0-1. (**B**) Inhibitory synapses (Teal-gephyrin) and dendritic spines (tdTomato) were labelled on distal apical dendrites of layer 2/3 neurons at P8 and P12. Teal-gephyrin puncta were observed on dendritic shafts (inhibitory shaft synapse; green arrowheads) and on dendritic spines (inhibitory spine synapse; blue arrowhead). (**C**) Quantification of dendritic spine, shaft gephyrin puncta, and spine gephyrin puncta densities across development *in vivo*. Spine density (red bars), shaft gephyrin puncta density (green bars), and spine gephyrin puncta density (blue bars) significantly increased between P6-8 (open bars; 2.52 ± 0.17, 0.86 ± 0.09, 0.25 ± 0.08) and P10-12 (filled bars; 5.41 ± 0.21, 1.61 ± 0.12, 1.21 ± 0.12). (P6-8: n=26 cells, 4 mice; P10-12: n=24 cells, 3 mice). $^{**}P < 0.01$. Error bars represent s.e.m.

Fig. S5

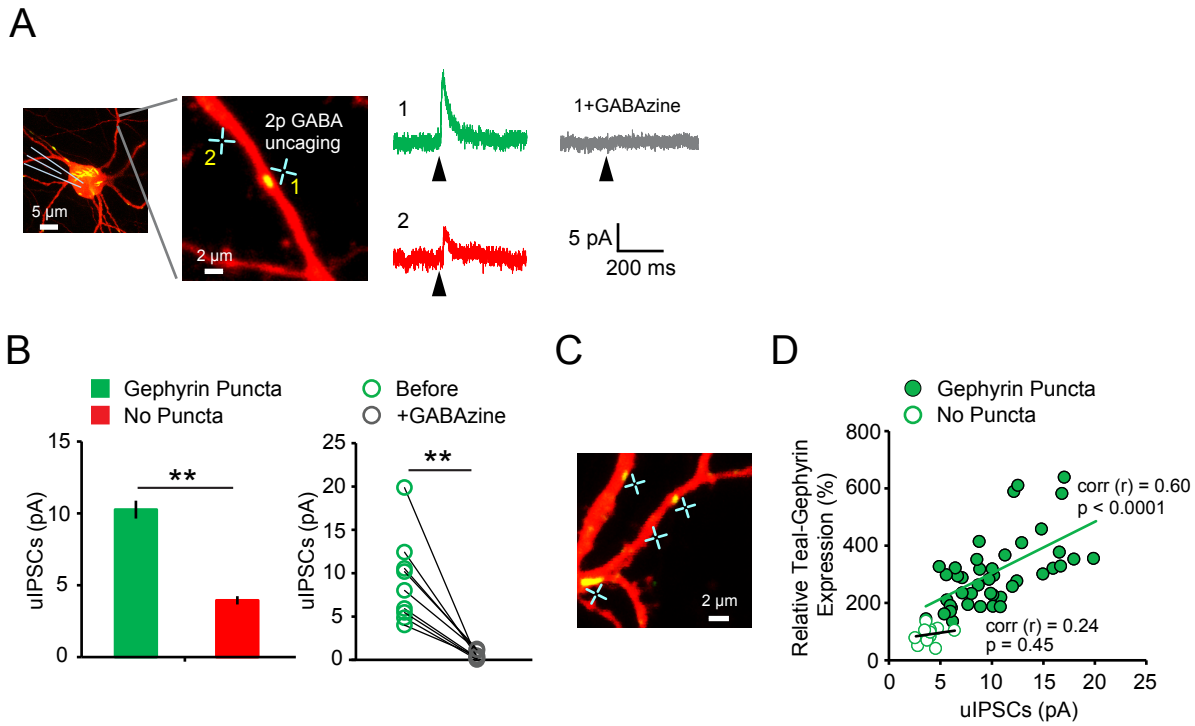

Fig. S5. Two-photon photolysis of CDNI-GABA at high spatiotemporal precision. (**A**) Left, a dendritic segment from a layer 2/3 pyramidal neuron coexpressing tdTomato (red) and Teal-gephyrin (green) in organotypic slice culture at EP14. Crosses indicate two-photon GABA uncaging spots (1 for gephyrin-positive; 2 for gephyrin-negative regions). Right, uIPSCs evoked by GABA uncaging (8-10 trials at 0.1 Hz) from both regions measured by whole-cell voltage clamp recording at +10 mV. A uIPSC trace in the presence of GABAzine is shown in gray. Arrowheads indicate time of GABA uncaging. (**B**) Left, summary graph of uIPSC amplitudes from gephyrin puncta (green bar; 10.27 ± 0.62pA, n=43 regions, 10 cells) and dendritic regions lacking gephyrin (red bar; 3.95 ± 0.28pA, n=12 regions). Right, uIPSCs from gephyrin puncta measured before and after GABAzine application (n=9 regions). (**C**) Examples of different sized gephyrin puncta that were targeted for GABA uncaging. (**D**) Scatter plot showing a positive correlation between gephyrin expression levels and the amplitude of uIPSCs (n=43, gephyrin puncta; n=12, no puncta). $^{**}P < 0.01$. Error bars represent s.e.m.

Fig. S6

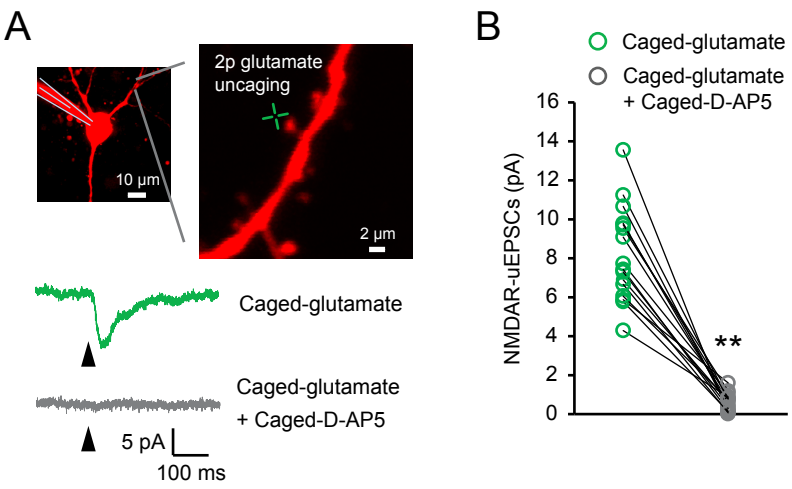

Fig. S6. Two-photon uncaging of NPEC-caged-D-AP5 completely abolishes NMDAR-mediated uEPSCs evoked by two-photon glutamate uncaging. (**A**) Top, a dendritic segment from a layer 2/3 pyramidal neuron filled with Alexa 594 (red) in organotypic slice culture at EP12. Cross indicates two-photon uncaging spot. Bottom, NMDAR-mediated uEPSCs evoked by glutamate uncaging (green, 8-10 trials at 0.1 Hz) measured by whole-cell voltage clamp recording at -65 mV in 0 mM Mg^{2+} ACSF containing NBQX. An NMDAR-mediated uEPSC trace after bath application of 0.5 mM NPEC-caged D-AP5 is shown in gray. Arrowheads indicate time of glutamate (top) and glutamte with D-AP5 (bottom) uncaging. (**B**) Summary graph of NMDAR-mediated uEPSCs from dendritic spines measured before (green circles, n=16 spines) and after NPEC-caged-D-AP5 application (gray circles, n=16 spines, 3 cells). $^{**}P < 0.01$.

Fig. S7

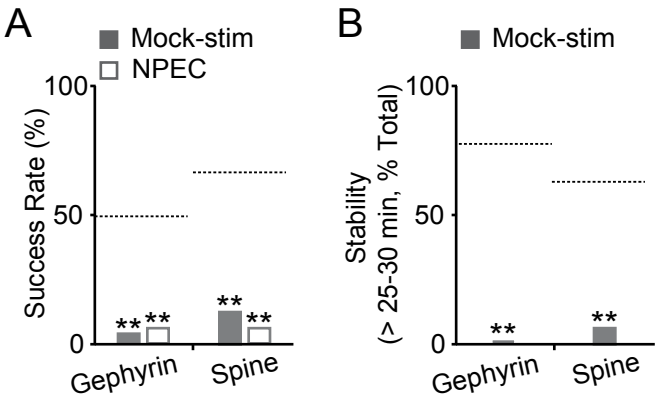

Fig. S7. Neither mock-stimulation nor uncaging of NPEC-caged-D-AP5 leads to successful induction. (**A**) Success rate of *de novo* gephyrin puncta and spine formation by mock-stimulation (n=34 trials, 15 cells) and NPEC HFU (n=17 trials, 8 cells). (**B**) Stability of newly formed gephyrin puncta (n=0 out of 4 new puncta) and dendritic spines (n=1 out of 16 new spines) by mock-stimulation. The dotted lines indicate the success rate (A) and stability (B) in control conditions with which statistical comparison was made. $^{**}P < 0.01$.

Fig. S8

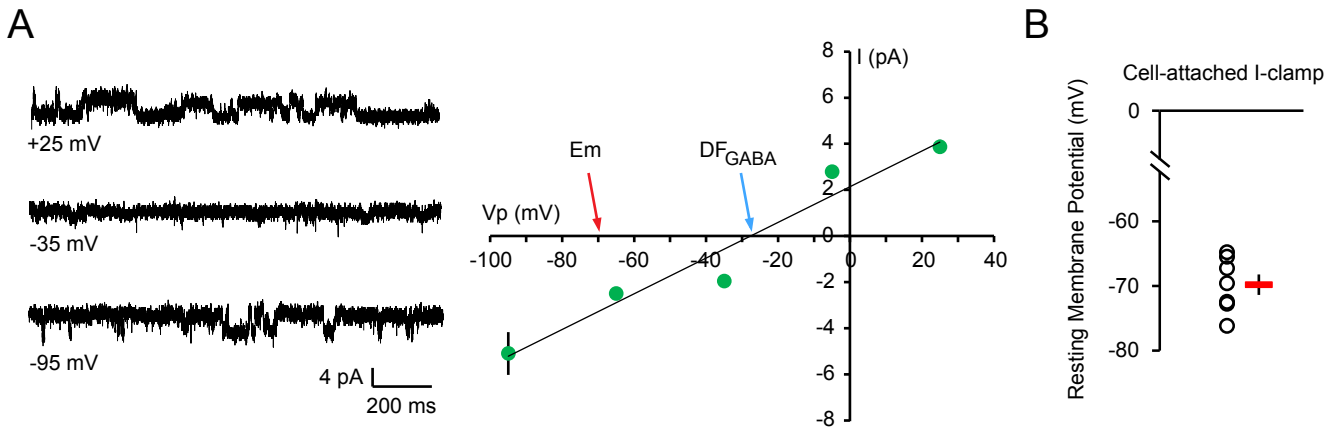

Fig. S8. Driving force of GABA-mediated currents. (**A**) Left, example traces of the cell-attached recordings of single $GABA_A$ receptor channels at different holding potentials from layer 2/3 pyramidal neurons in organotypic slice culture at EP7-8. Right, I-V relationships of the $GABA_A$ single channels. Driving force of GABA-mediated currents (DF_{GABA}; -27.6mV) was measured by calculating the intercept of the linear fit of the I-V curve with the x-axis (n=23 cells). (**B**) Summary plot of the resting membrane potential (Em; -69.8 ± 1.6mV, n=7 cells) of layer 2/3 pyramidal neurons in organotypic slice culture at EP7-8 measured by cell-attached current-clamp recordings. Em = -69.8 ± 1.6mV, DF_{GABA} = -27.6mV. The reversal potential for GABA currents is -42.3 ± 1.6mV in layer 2/3 pyramidal neurons at EP7-8. Error bars represent s.e.m.

Fig. S9

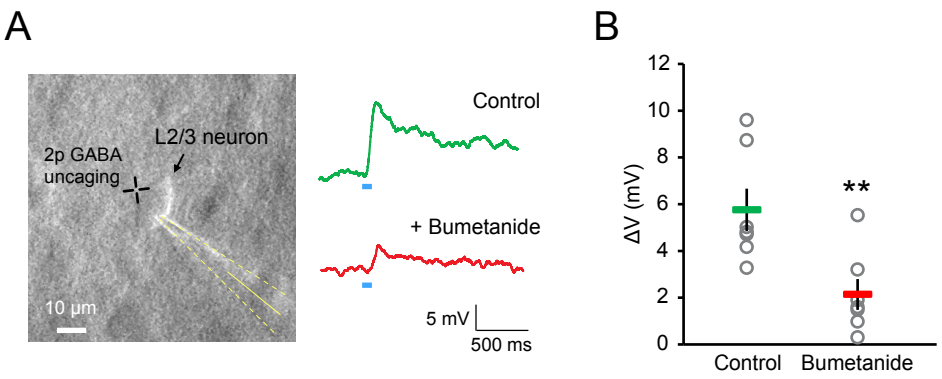

Fig. S9. GABA-mediated depolarization in immature neocortical neurons. (A) Left, a DIC image of an organotypic cortical slice culture at EP6 showing cell-attached current-clamp recording from a layer 2/3 pyramidal neuron. Cross indicates two-photon GABA uncaging spot. Right, GABA uncaging (1 pulse of 50-ms duration)-induced depolarization in the absence (top, green) and presence (bottom, red) of bumetanide (10 µM) measured by cell-attached current-clamp recordings. Blue bars indicate time of GABA uncaging. (**B**) Summary graph of GABA-mediated depolarization measured before (left, green bar; 5.8 ± 0.9mV, n=7 cells) and after bumetanide application (right, red bar; 2.1 ± 0.7mV, n=7 cells). Bath application of bumetanide (> 1 hr) significantly reduced depolarizing action of GABA. $^{**}P < 0.01$. Error bars represent s.e.m.

Fig. S10

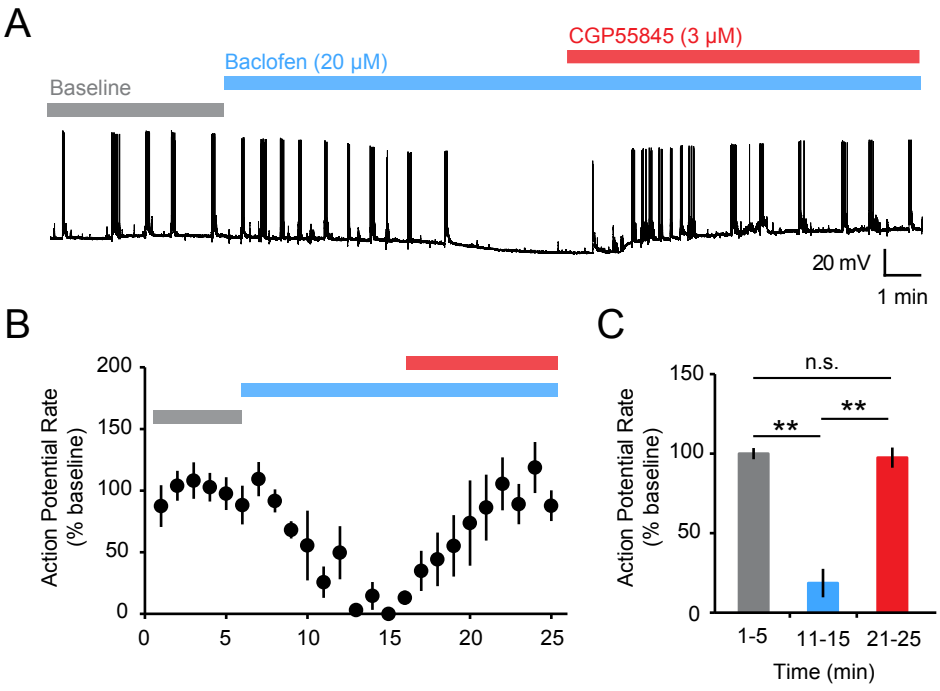

Fig. S10. CGP55845 effectively reverses baclofen-mediated reduction in the firing rate of action potentials. (**A**) Example traces showing spontaneous action potentials measured by whole-cell current clamp recordings from layer 2/3 pyramidal neurons of organotypic cortical slices at 9-10 DIV. Baseline firing rate (gray bar) was gradually but significantly reduced after bath application of baclofen (blue bar) at t=6 min. This effect was reversed by addition of CGP55845 (red bar) in the bath at t=16 min. (**B**) Time course of the action potential firing rates following application of CGP55845 (3 µM; red bar) in layer 2/3 neurons of cortical slices pretreated with baclofen (20 µM; blue bar). (**C**) The baseline firing rate (gray bar; 100 ± 4%) was significantly decreased after a 5- to 10 min baclofen application (blue bar; 19 ± 9%). Bath application of CGP55845 (red bar; 97 ± 6%) completely reversed baclofen activation of $GABA_B$ receptors (n=5 cells). $^{**}P < 0.01$. Error bars represent s.e.m.; n.s., not significant.

Fig. S11

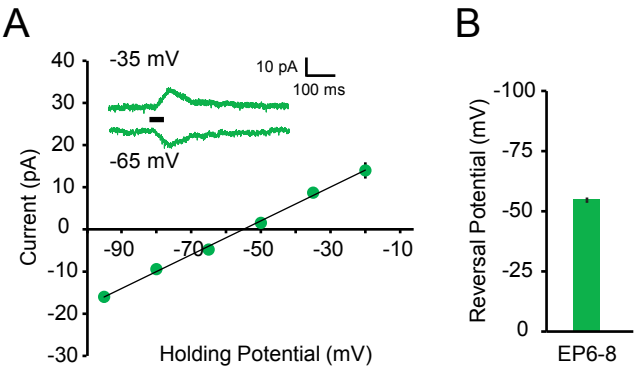

Fig. S11. Chloride reversal potentials estimated by whole-cell patch clamp recordings. (**A**) Current-voltage (I-V) curves measured by whole-cell patch clamp recordings from layer 2/3 neurons in organotypic slice culture at EP6-8. Recordings were made at several hold potentials, and the chloride reversal potentials (E_{Cl^-}) were estimated by calculating the intercept of the linear fit of the I-V curve with the x-axis. Inset: averaged GABA uncaging-evoked uIPSCs (1 pulse of 50-ms duration, 6-8 trials). Black bar indicates time of GABA uncaging. (**B**) Summary graph of E_{Cl^-} measured at EP6-8 (-55.0 ± 0.96mV, n=24 cells). Related to Figure 3A to F.

Fig. S12

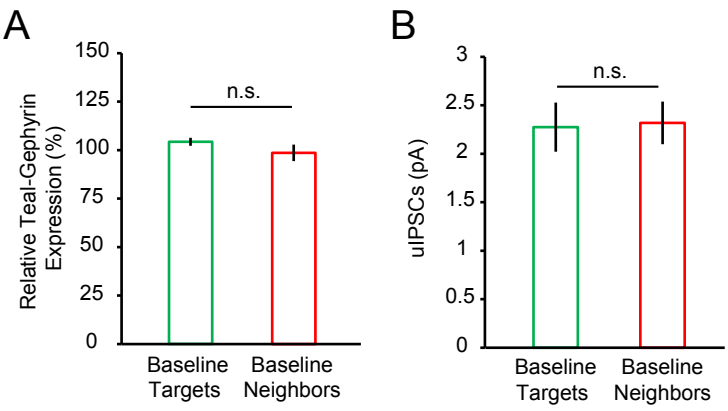

Fig. S12. Unbiased selection of HFU locations. (**A**) Teal-gephyrin expression levels at targets (green bar; 104 ± 2%) were comparable to those of neighbors (red bar; 99 ± 4%, $P = 0.24$) at the start of the study. (**B**) Baseline uncaging-evoked inhibitory postsynaptic currents (uIPSCs) from targets (green bar; 2.27 ± 0.25pA) were not significantly different from those of neighboring regions (red bar; 2.32 ± 0.22pA, n=12 cells, $P = 0.89$). Error bars represent s.e.m.; n.s., not significant.

Fig. S13

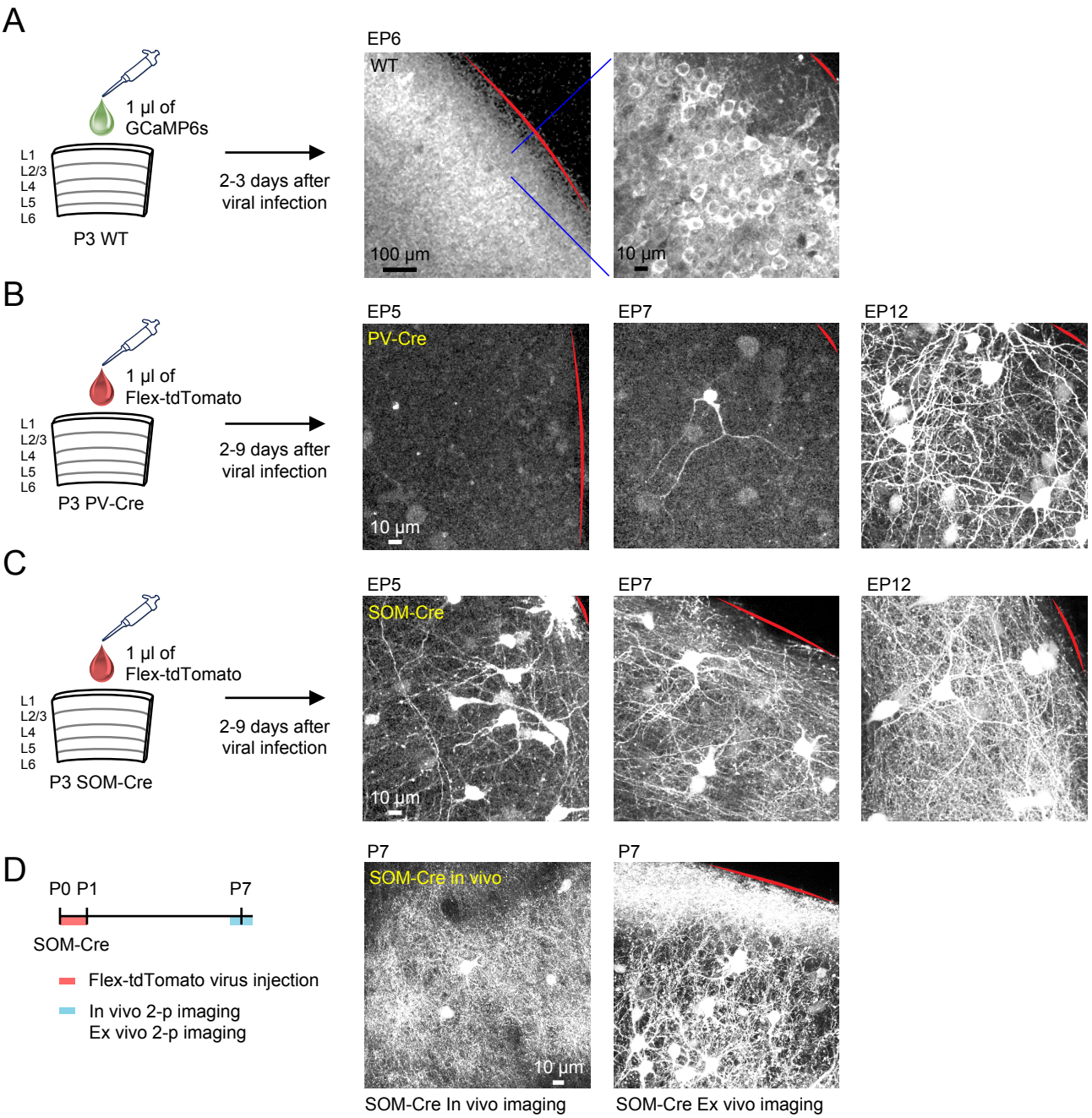

Fig. S13. Age-dependent expression of Flex-tdTomato in PV- and SOM-Cre mice. (**A**) Schematic showing GCaMP6s virus infection on WT slice at P3. Validation of virus infection on organotypic cortical slice cultures using GCaMP6s. Large-scale viral infection was highly efficient on cortical slices within 2-3 days of GCaMP6s virus infection. (**B**) Schematic showing Flex-tdTomato virus infection on PV-Cre slice at P3. Two-photon images of organotypic cortical slices of PV-Cre mouse infected by Flex-tdTomato virus. Very little PV expression was observed in young slices (EP5-7). Clear axonal arborizations of PV interneurons were observed at EP12, several days later than what were seen in SOM-Cre slices. (**C**) Schematic showing Flex-tdTomato virus infection on SOM-Cre slice at P3. Two-photon images of organotypic cortical slices of SOM-Cre mouse infected by Flex-tdTomato virus. Clear tdTomato expression was observed at early stages (EP5-7). tdTomato-expressing SOM interneurons showed widely spread and highly dense axonal arborizations, which were continued to be increased through to EP12. (**D**) Experimental timeline. P, postnatal day. AAV-CAG-Flex-tdTomato was injected into somatosensory cortex of SOM-Cre at P0-1. Clear axonal arborizations of SOM interneurons were observed *in vivo* and in acute cortical brain slices.

Fig. S14

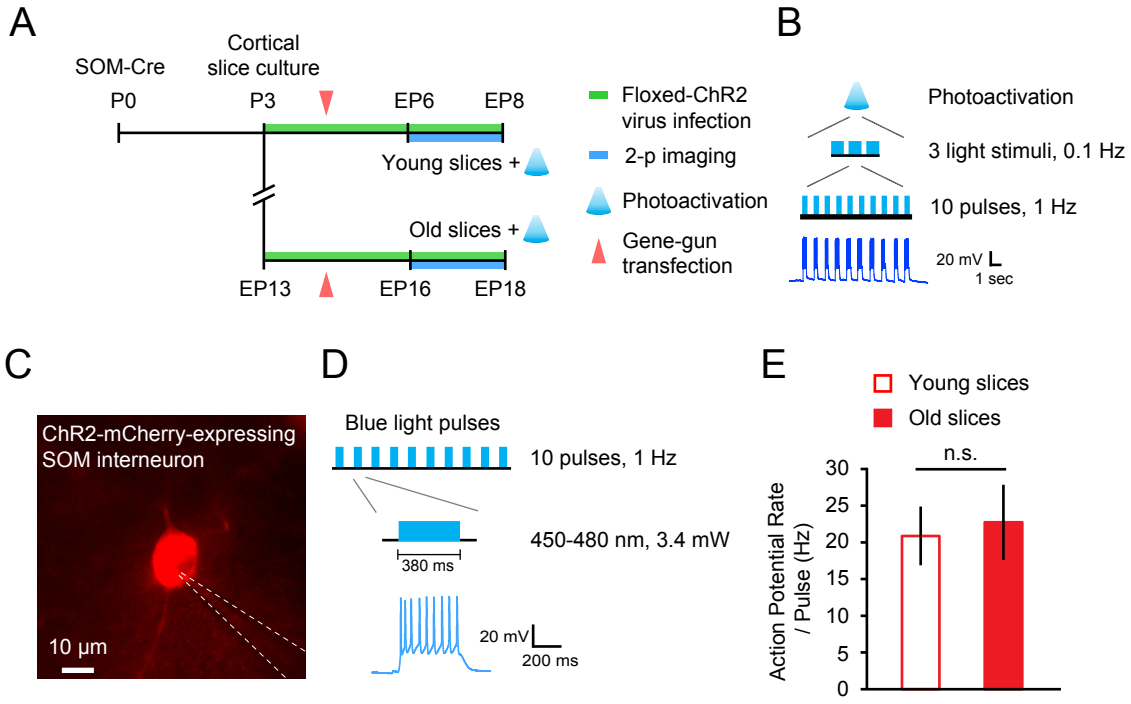

Fig. S14. Photoactivation protocol and validation of optogenetic stimulation in ChR2-expressing SOM interneurons. (**A**) Schematic cartoon of the experimental protocol. P, postnatal day. EP, equivalent postnatal day (postnatal day at slice culturing + days in vitro). (**B**) Three trains of optical stimuli delivered at 0.1 Hz for photoactivation. Each optical stimulus consisted of ten pulses of 380-ms duration delivered at 1 Hz and evoked a train of action potentials. (**C**) Representative image of a cortical somatostatin interneuron expressing ChR2-mCherry recorded by whole-cell current clamp mode. (**D**) Blue light stimulus consisted of 10 pulses (450-480 nm; 3.4 mW at the sample) of 380-ms duration delivered at 1 Hz. Each pulse of blue light elicited a train of action potentials at an average rate of ~20 Hz. (**E**) Firing rates evoked by the optical stimulus were not significantly different between young (open bar; 20.88 ± 4.01Hz, n=5 cells) and old (filled bar; 22.74 ± 5.12Hz, n=6 cells, $P = 0.79$) neurons. Error bars represent s.e.m.; n.s., not significant.

Fig. S15

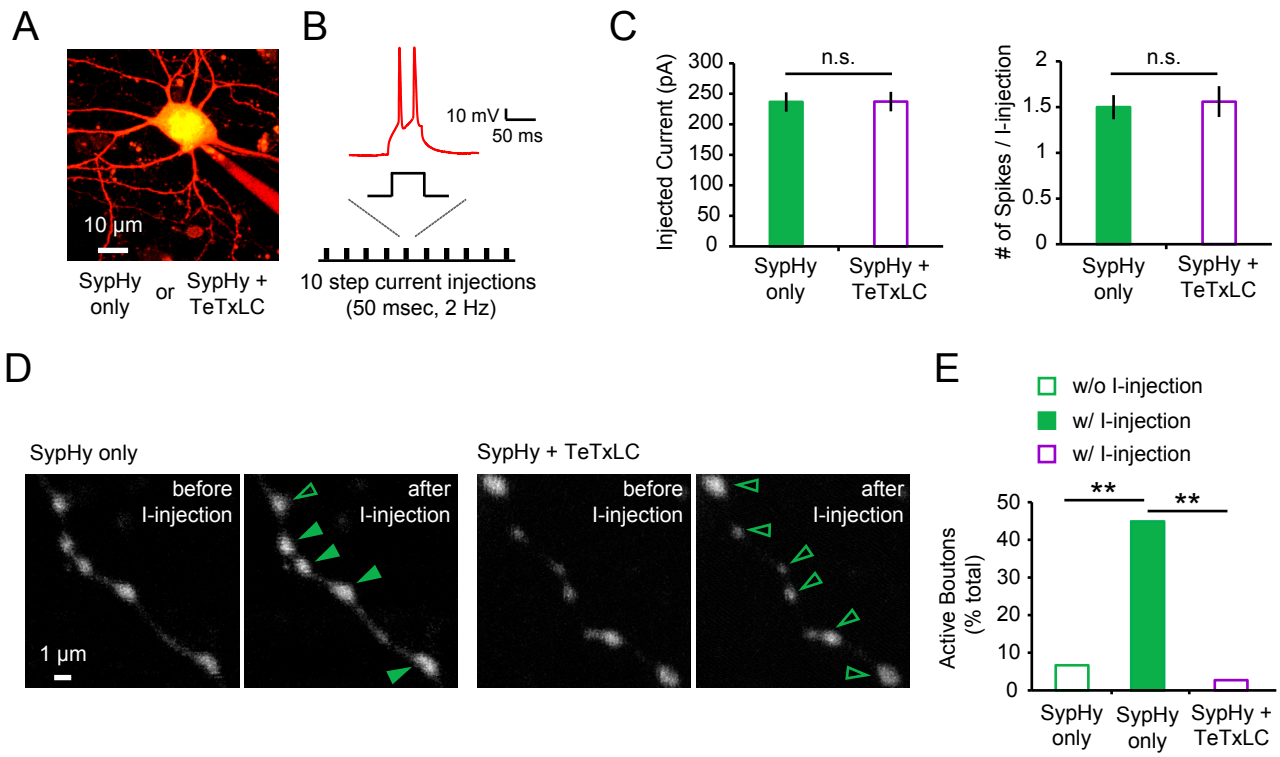

Fig. S15. Tetanus toxin light-chain (TeTxLC) efficiently blocks synaptic vesicle release. (**A**) Two-photon image of whole-cell recording from a layer 2/3 pyramidal neuron coexpressing tdTomato, SypHy, Flex-tetanus toxin light-chain, and Cre. (**B**) A stimulus train of action potentials was evoked by 10 step current injections (200-300 pA, 50 ms) delivered at 2 Hz. (**C**) The amount of current required to elicit action potential firing (left panel; SypHy only: 236.67 ± 15.85pA; SypHy+TeTxLC: 237.14 ± 15.99pA; $P = 0.98$) and the number of action potentials evoked by the step current injections (right panel; SypHy only: 1.50 ± 0.13; SypHy+TeTxLC: 1.56 ± 0.17; $P = 0.79$) were not significantly different between cells expressing SypHy alone (filled green bars; n=6 cells) and those coexpressing SypHy and TeTxLC (open purple bars; n=7 cells). (**D**) Fluorescence of SypHy increased in the majority of the axonal boutons from a SypHy only expressing neuron after current injections (left panel, filled green arrowheads), but not in a SypHy and TeTxLC cotransfected neuron (right panel, open green arrowheads). (**E**) Current injections significantly increased the number of active boutons in cells expressing SypHy alone (filled green bar; n=52 active boutons / 116 boutons, 6 cells) relative to baseline fluorescence changes (open green bar; n=7 active boutons / 105 boutons, 5 cells) and cells coexpressing SypHy and TeTxLC (open purple bar; n=4 active boutons / 148 boutons, 7 cells). Note that axonal boutons exhibiting more than 18% increase in $\Delta F/F_0$ (average 2 SDs of $\Delta F/F_0$ at resting state, n=5 cells) were considered as active boutons. $^{**}P < 0.01$. Error bars represent s.e.m.; n.s., not significant.

Fig. S16

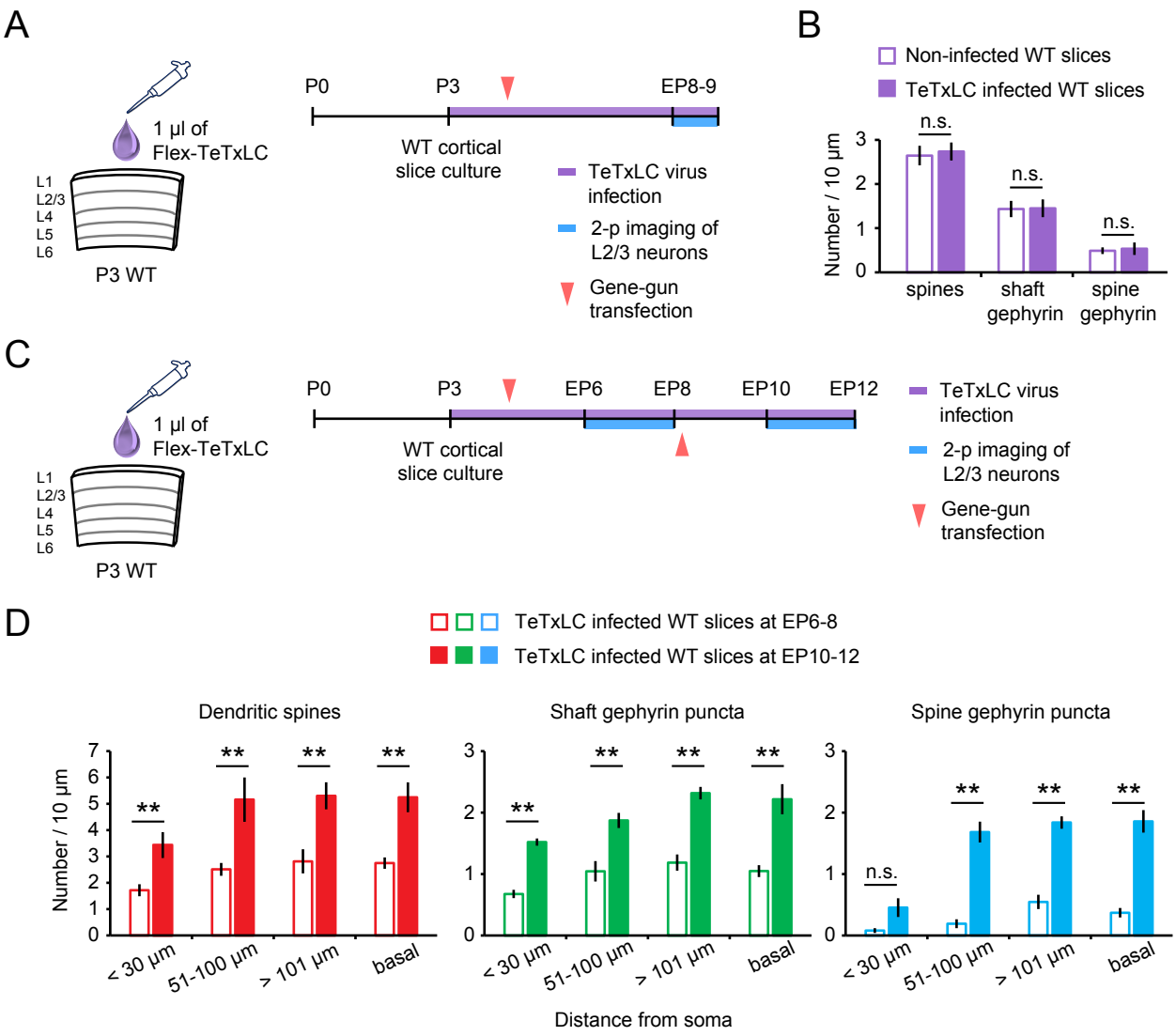

Fig. S16. Flex-TeTxLC viral infection does not affect excitatory and inhibitory synapses of layer 2/3 pyramidal neurons in wild-type slices. (**A**) Schematic showing Flex-TeTxLC virus infection on WT slice at P3. Experimental timeline. P, postnatal day. EP, equivalent postnatal day (postnatal day at slice culturing + days *in vitro*). (**B**) The density of dendritic spines (control: 2.64 ± 0.22; TeTxLC: 2.74 ± 0.20; $P = 0.77$), shaft gephyrin puncta (control: 1.43 ± 0.18; TeTxLC: 1.45 ± 0.20; $P = 0.95$), and spine gephyrin puncta (control: 0.49 ± 0.08; TeTxLC: 0.54 ± 0.14; $P = 0.77$) was not significantly different between cells in non-infected (open bars; n=8 cells) and TeTxLC infected (filled bars; n=7 cells) wild-type slices. (**C**) Schematic showing Flex-TeTxLC virus infection on WT slice at P3. Experimental timeline. (**D**) Quantitative analysis of the density of dendritic spines (red bars; EP6-8: <30µm, 51-100µm, >101µm, basal: 1.72 ± 0.23, 2.51 ± 0.24, 2.81 ± 0.46, 2.75 ± 0.22; EP10-12: 3.43 ± 0.49, 5.16 ± 0.84, 5.30 ± 0.51, 5.25 ± 0.57), shaft gephyrin puncta (green bars; EP6-8: 0.68 ± 0.07, 1.04 ± 0.17, 1.19 ± 0.13, 1.05 ± 0.10; EP10-12: 1.52 ± 0.06, 1.87 ± 0.12, 2.32 ± 0.10, 2.22 ± 0.25), and spine gephyrin puncta (blue bars; EP6-8: 0.08 ± 0.04, 0.19 ± 0.07, 0.55 ± 0.12, 0.37 ± 0.08; EP10-12: 0.45 ± 0.15, 1.68 ± 0.17, 1.84 ± 0.10, 1.86 ± 0.18) on different dendritic branches showed a significant increase between EP6-8 (open bars; n=7 cells) and EP10-12 (filled bars; n=6 cells) in WT cultures infected by TeTxLC virus, consistent with the previous findings on non-infected WT slices (Fig. S2, B to D). $^{**}P < 0.01$. Error bars represent s.e.m.; n.s., not significant.

Fig. S17

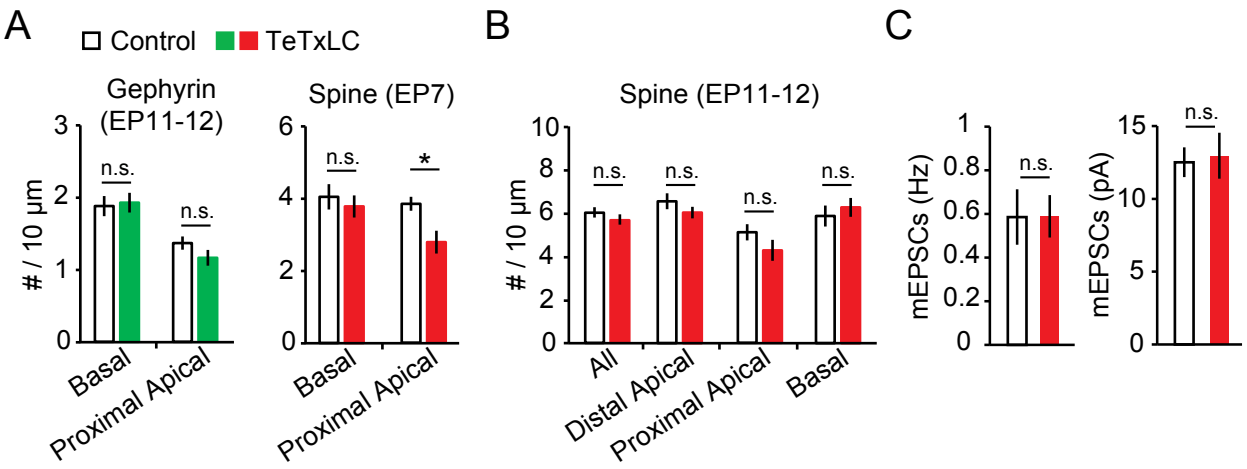

Fig. S17. Branch-specific and age-dependent effects of TeTxLC-expressing somatostatin interneurons on layer 2/3 neurons. (**A** and **B**) Quantitative analysis of the density of gephyrin puncta and spines from control (n=4 dendrites/cell, 13 cells) and TeTxLC-infected (n=7 dendrites/cell, 15 cells) slices at EP11-12 and at EP7 (control: n=4 dendrites/cell, 8 cells; TeTxLC: n=4 dendrites/cell, 10 cells). (**C**) Quantitative analysis of the frequency and amplitude of mEPSCs (control: n=12; TeTxLC: n=13) at EP11-12. *$P < 0.05$; Error bars represent s.e.m.; n.s., not significant.

Fig. S18

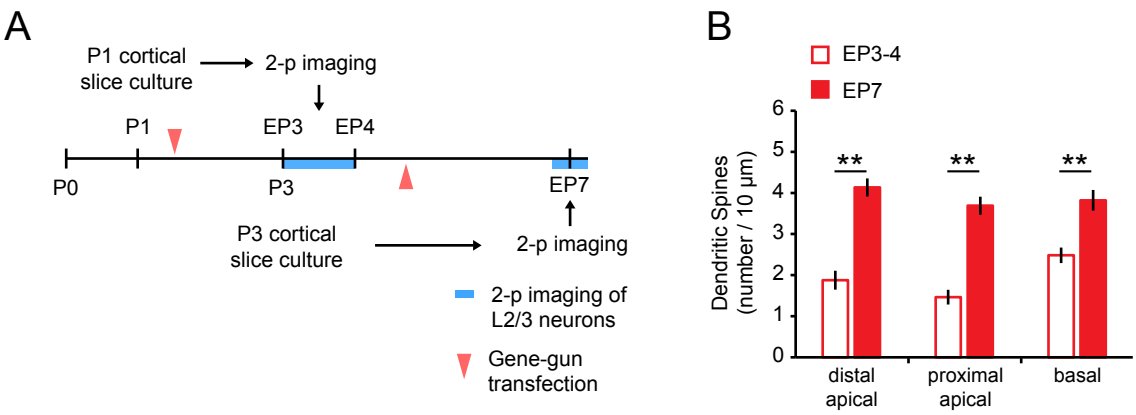

Fig. S18. Increase in dendritic spine density on layer 2/3 pyramidal neurons in the somatosensory cortex during the first week after birth. (**A**) Experimental timeline. P, postnatal day. EP, equivalent postnatal day (postnatal day at slice culturing + days *in vitro*). (**B**) Spine density significantly increased between EP3-4 (open bars; distal, proximal, basal: 1.88 ± 0.23, 1.46 ± 0.18, 2.48 ± 0.19, n=8 cells) and EP7 (filled bars; 4.13 ± 0.22, 3.69 ± 0.22, 3.82 ± 0.25, n=11 cells). $^{**}P < 0.01$. Error bars represent s.e.m.

Fig. S19

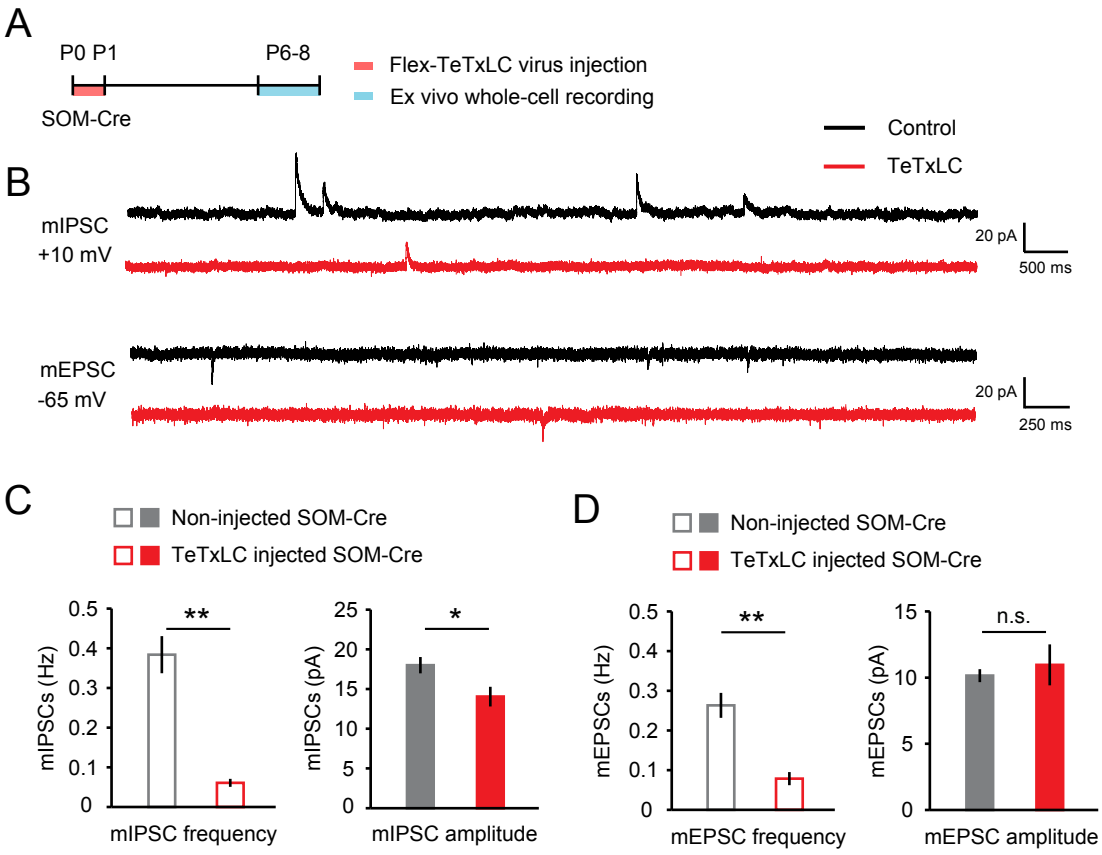

Fig. S19. ***In vivo*** **expression of TeTxLC in somatostatin interneurons significantly reduces the frequency of both mIPSCs and mEPSCs in layer 2/3 neurons.** (**A**) Experimental timeline. P, postnatal day. AAV-CAG-Flex-tetanus toxin light-chain was injected into somatosensory cortex of SOM-Cre at P0-1. (**B**) Representative traces of mIPSCs (top, at +10 mV) and mEPSCs (bottom, at -65 mV) measured by whole-cell patch clamp recordings from layer 2/3 neurons in acute cortical brain slices of non-injected control (black) and TeTxLC-injected (red) SOM-Cre at P7. (**C**) Both the frequency (open bars; control: 0.38 ± 0.05Hz; TeTxLC: 0.06 ± 0.01Hz) and amplitude (filled bars; control: 18.01 ± 1.03pA; TeTxLC: 14.05 ± 1.25pA) of mIPSCs were significantly different between control (gray bars; n=12 cells) and TeTxLC-injected SOM-Cre (red bars; n=10 cells). (**D**) The frequency (open bars; control: 0.26 ± 0.03Hz; TeTxLC: 0.08 ± 0.02Hz), but not amplitude (filled bars; control: 10.15 ± 0.49pA; TeTxLC: 10.96 ± 1.55pA), of mEPSCs was significantly different between control (gray bars; n=11 cells) and TeTxLC-injected SOM-Cre (red bars; n=11 cells). **P* < 0.05; ***P* < 0.01. Error bars represent s.e.m.; n.s., not significant.

References

1. T. Branco, B. A. Clark, M. Häusser, Dendritic discrimination of temporal input sequences in cortical neurons. *Science* **329**, 1671–1675 (2010). Medline doi:10.1126/science.1189664

2. C. Q. Chiu, G. Lur, T. M. Morse, N. T. Carnevale, G. C. Ellis-Davies, M. J. Higley, Compartmentalization of GABAergic inhibition by dendritic spines. *Science* **340**, 759–762 (2013). Medline doi:10.1126/science.1234274

3. T. Hayama, J. Noguchi, S. Watanabe, N. Takahashi, A. Hayashi-Takagi, G. C. Ellis-Davies, M. Matsuzaki, H. Kasai, GABA promotes the competitive selection of dendritic spines by controlling local Ca^{2+} signaling. *Nat. Neurosci.* **16**, 1409–1416 (2013). Medline doi:10.1038/nn.3496

4. A. Losonczy, J. C. Magee, Integrative properties of radial oblique dendrites in hippocampal CA1 pyramidal neurons. *Neuron* **50**, 291–307 (2006). Medline doi:10.1016/j.neuron.2006.03.016

5. N. Spruston, Pyramidal neurons: Dendritic structure and synaptic integration. *Nat. Rev. Neurosci.* **9**, 206–221 (2008). Medline doi:10.1038/nrn2286

6. P. Caroni, F. Donato, D. Muller, Structural plasticity upon learning: Regulation and functions. *Nat. Rev. Neurosci.* **13**, 478–490 (2012). Medline doi:10.1038/nrn3258

7. A. M. Hamilton, W. C. Oh, H. Vega-Ramirez, I. S. Stein, J. W. Hell, G. N. Patrick, K. Zito, Activity-dependent growth of new dendritic spines is regulated by the proteasome. *Neuron* **74**, 1023–1030 (2012). Medline doi:10.1016/j.neuron.2012.04.031

8. Y. Kozorovitskiy, A. Saunders, C. A. Johnson, B. B. Lowell, B. L. Sabatini, Recurrent network activity drives striatal synaptogenesis. *Nature* **485**, 646–650 (2012). Medline doi:10.1038/nature11052

9. H. B. Kwon, B. L. Sabatini, Glutamate induces de novo growth of functional spines in developing cortex. *Nature* **474**, 100–104 (2011). Medline doi:10.1038/nature09986

10. J. L. Chen, K. L. Villa, J. W. Cha, P. T. So, Y. Kubota, E. Nedivi, Clustered dynamics of inhibitory synapses and dendritic spines in the adult neocortex. *Neuron* **74**, 361–373 (2012). Medline doi:10.1016/j.neuron.2012.02.030

11. D. van Versendaal, R. Rajendran, M. H. Saiepour, J. Klooster, L. Smit-Rigter, J. P. Sommeijer, C. I. De Zeeuw, S. B. Hofer, J. A. Heimel, C. N. Levelt, Elimination of inhibitory synapses is a major component of adult ocular dominance plasticity. *Neuron* **74**, 374–383 (2012). Medline doi:10.1016/j.neuron.2012.03.015

12. M. Matsuzaki, T. Hayama, H. Kasai, G. C. Ellis-Davies, Two-photon uncaging of gamma-aminobutyric acid in intact brain tissue. *Nat. Chem. Biol.* **6**, 255–257 (2010). Medline doi:10.1038/nchembio.321

13. T. Kim, W. C. Oh, J. H. Choi, H. B. Kwon, Emergence of functional subnetworks in layer 2/3 cortex induced by sequential spikes in vivo. *Proc. Natl. Acad. Sci. U.S.A.* **113**, E1372–E1381 (2016). Medline doi:10.1073/pnas.1513410113

14. Y. Ben-Ari, The GABA excitatory/inhibitory developmental sequence: A personal journey. *Neuroscience* **279**, 187–219 (2014). Medline doi:10.1016/j.neuroscience.2014.08.001

15. C. Lüscher, L. Y. Jan, M. Stoffel, R. C. Malenka, R. A. Nicoll, G protein-coupled inwardly rectifying K^+ channels (GIRKs) mediate postsynaptic but not presynaptic transmitter actions in hippocampal neurons. *Neuron* **19**, 687–695 (1997). Medline doi:10.1016/S0896-6273(00)80381-5

16. J. Kirsch, H. Betz, Glycine-receptor activation is required for receptor clustering in spinal neurons. *Nature* **392**, 717–720 (1998). Medline doi:10.1038/33694

17. T. A. Hage, Z. M. Khaliq, Tonic firing rate controls dendritic Ca^{2+} signaling and synaptic gain in substantia nigra dopamine neurons. *J. Neurosci.* **35**, 5823–5836 (2015). Medline doi:10.1523/JNEUROSCI.3904-14.2015

18. G. W. Knott, A. Holtmaat, L. Wilbrecht, E. Welker, K. Svoboda, Spine growth precedes synapse formation in the adult neocortex in vivo. *Nat. Neurosci.* **9**, 1117–1124 (2006). Medline doi:10.1038/nn1747

19. U. V. Nägerl, G. Köstinger, J. C. Anderson, K. A. Martin, T. Bonhoeffer, Protracted synaptogenesis after activity-dependent spinogenesis in hippocampal neurons. *J. Neurosci.* **27**, 8149–8156 (2007). Medline doi:10.1523/JNEUROSCI.0511-07.2007

20. K. Zito, V. Scheuss, G. Knott, T. Hill, K. Svoboda, Rapid functional maturation of nascent dendritic spines. *Neuron* **61**, 247–258 (2009). Medline doi:10.1016/j.neuron.2008.10.054

21. R. Batista-Brito, R. Machold, C. Klein, G. Fishell, Gene expression in cortical interneuron precursors is prescient of their mature function. *Cereb. Cortex* **18**, 2306–2317 (2008). Medline doi:10.1093/cercor/bhm258

22. A. J. Murray, J. F. Sauer, G. Riedel, C. McClure, L. Ansel, L. Cheyne, M. Bartos, W. Wisden, P. Wulff, Parvalbumin-positive CA1 interneurons are required for spatial working but not for reference memory. *Nat. Neurosci.* **14**, 297–299 (2011). Medline doi:10.1038/nn.2751

23. S. X. Chen, A. N. Kim, A. J. Peters, T. Komiyama, Subtype-specific plasticity of inhibitory circuits in motor cortex during motor learning. *Nat. Neurosci.* **18**, 1109–1115 (2015). Medline doi:10.1038/nn.4049

24. J. Cichon, W. B. Gan, Branch-specific dendritic Ca^{2+} spikes cause persistent synaptic plasticity. *Nature* **520**, 180–185 (2015). Medline doi:10.1038/nature14251

25. M. Cane, B. Maco, G. Knott, A. Holtmaat, The relationship between PSD-95 clustering and spine stability in vivo. *J. Neurosci.* **34**, 2075–2086 (2014). Medline doi:10.1523/JNEUROSCI.3353-13.2014

26. B. Dejanovic, M. Semtner, S. Ebert, T. Lamkemeyer, F. Neuser, B. Lüscher, J. C. Meier, G. Schwarz, Palmitoylation of gephyrin controls receptor clustering and plasticity of GABAergic synapses. *PLOS Biol.* **12**, e1001908 (2014). Medline doi:10.1371/journal.pbio.1001908

27. C. E. Flores, I. Nikonenko, P. Mendez, J. M. Fritschy, S. K. Tyagarajan, D. Muller, Activity-dependent inhibitory synapse remodeling through gephyrin phosphorylation. *Proc. Natl. Acad. Sci. U.S.A.* **112**, E65–E72 (2015). Medline doi:10.1073/pnas.1411170112

28. Z. J. Huang, Activity-dependent development of inhibitory synapses and innervation pattern: Role of GABA signalling and beyond. *J. Physiol.* **587**, 1881–1888 (2009). Medline doi:10.1113/jphysiol.2008.168211

29. M. Miller, A. Peters, Maturation of rat visual cortex. II. A combined Golgi-electron microscope study of pyramidal neurons. *J. Comp. Neurol.* **203**, 555–573 (1981). Medline doi:10.1002/cne.902030402

30. L. Stoppini, P. A. Buchs, D. Muller, A simple method for organotypic cultures of nervous tissue. *J. Neurosci. Methods* **37**, 173–182 (1991). Medline doi:10.1016/0165-0270(91)90128-M

31. H. B. Kwon, Y. Kozorovitskiy, W. J. Oh, R. T. Peixoto, N. Akhtar, J. L. Saulnier, C. Gu, B. L. Sabatini, Neuroligin-1-dependent competition regulates cortical synaptogenesis and synapse number. *Nat. Neurosci.* **15**, 1667–1674 (2012). Medline doi:10.1038/nn.3256

32. B. Granseth, B. Odermatt, S. J. Royle, L. Lagnado, Clathrin-mediated endocytosis is the dominant mechanism of vesicle retrieval at hippocampal synapses. *Neuron* **51**, 773–786 (2006). Medline doi:10.1016/j.neuron.2006.08.029

33. T. W. Chen, T. J. Wardill, Y. Sun, S. R. Pulver, S. L. Renninger, A. Baohan, E. R. Schreiter, R. A. Kerr, M. B. Orger, V. Jayaraman, L. L. Looger, K. Svoboda, D. S. Kim, Ultrasensitive fluorescent proteins for imaging neuronal activity. *Nature* **499**, 295–300 (2013). Medline doi:10.1038/nature12354

34. W. C. Oh, T. C. Hill, K. Zito, Synapse-specific and size-dependent mechanisms of spine structural plasticity accompanying synaptic weakening. *Proc. Natl. Acad. Sci. U.S.A.* **110**, E305–E312 (2013). Medline doi:10.1073/pnas.1214705110

35. G. F. Woods, W. C. Oh, L. C. Boudewyn, S. K. Mikula, K. Zito, Loss of PSD-95 enrichment is not a prerequisite for spine retraction. *J. Neurosci.* **31**, 12129–12138 (2011). Medline doi:10.1523/JNEUROSCI.6662-10.2011

36. R. Yasuda, E. A. Nimchinsky, V. Scheuss, T. A. Pologruto, T. G. Oertner, B. L. Sabatini, K. Svoboda, Imaging calcium concentration dynamics in small neuronal compartments. *Sci. STKE* **2004**, pl5 (2004). Medline